Supplementary Information

Cortical VIP neurons locally control the gain but globally control the coherence of gamma band rhythms

Julia Veit, Gregory Handy, Daniel P. Mossing, Brent Doiron and Hillel Adesnik

This file includes:

Supplementary Figures S1-S6
Methods S1-S2
Table S1-S2

Figure S1 – related to Figure 1

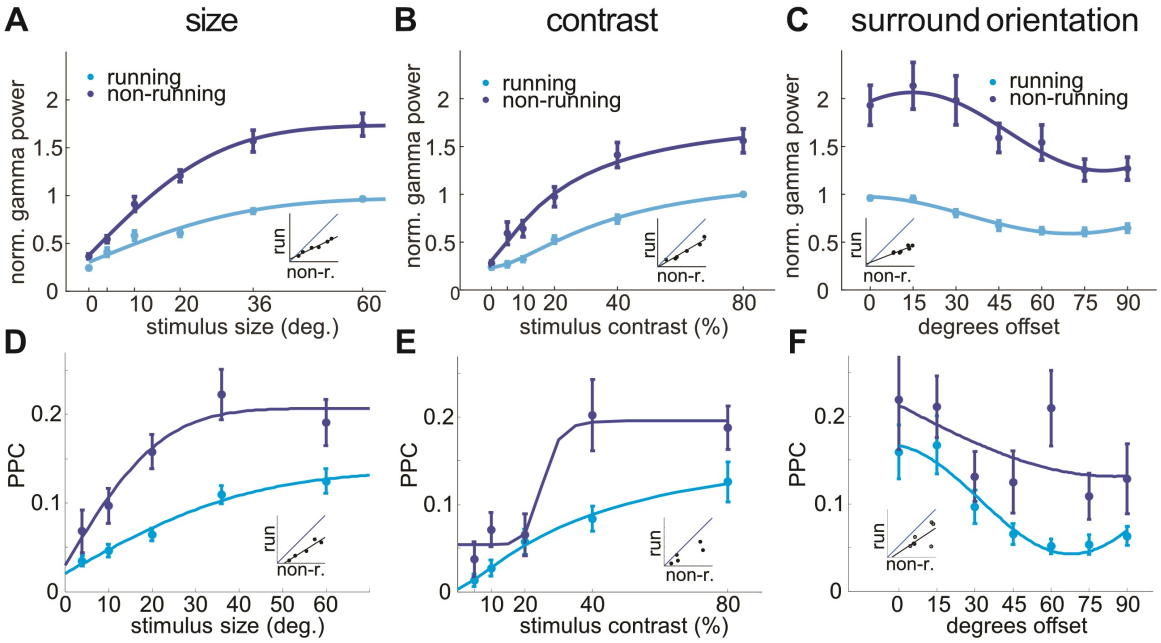

Figure S1: Gamma power and phase locking depend on behavioral state. A: Average normalized gamma power during running (light blue) and quiescence (dark blue) versus stimulus size (n = 17 mice, 2-way-ANOVA: main effect of size: $p < 0.001$; main effect of running $p < 0.001$; interaction: $p < 0.001$). **B:** Average normalized gamma power during running and quiescence versus stimulus contrast (n = 18 mice, 2-way ANOVA: main effect of contrast: $p < 0.001$; main effect of running: $p < 0.001$; interaction: $p = 0.008$). **C:** Average normalized gamma power during running and quiescence versus relative surround orientation (n = 10 mice, 2-way ANOVA: main effect of orientation: $p < 0.001$; main effect of running: $p < 0.001$; interaction: $p = 0.24$) **D:** Average PPC during running (light blue) and quiescence (dark blue) versus stimulus size (n = 87 units, 2-way-ANOVA: main effect of size: $p<0.001$; main effect of running: $p < 0.001$; interaction: $p = 0.36$). **E:** Average PPC during running and quiescence versus stimulus contrast (n = 29 units, 2-way-ANOVA: main effect of contrast: $p < 0.001$; main effect of running: $p < 0.001$; interaction: $p = 0.11$). **F:** Average PPC during running and quiescence versus relative surround orientation (n = 28 units, 2-way-ANOVA: main effect of orientation: $p= 0.001$; main effect of running: $p<0.001$; interaction: $p = 0.54$). Error bars in all plots represent s.e.m.

Figure S2 – related to Figure 1

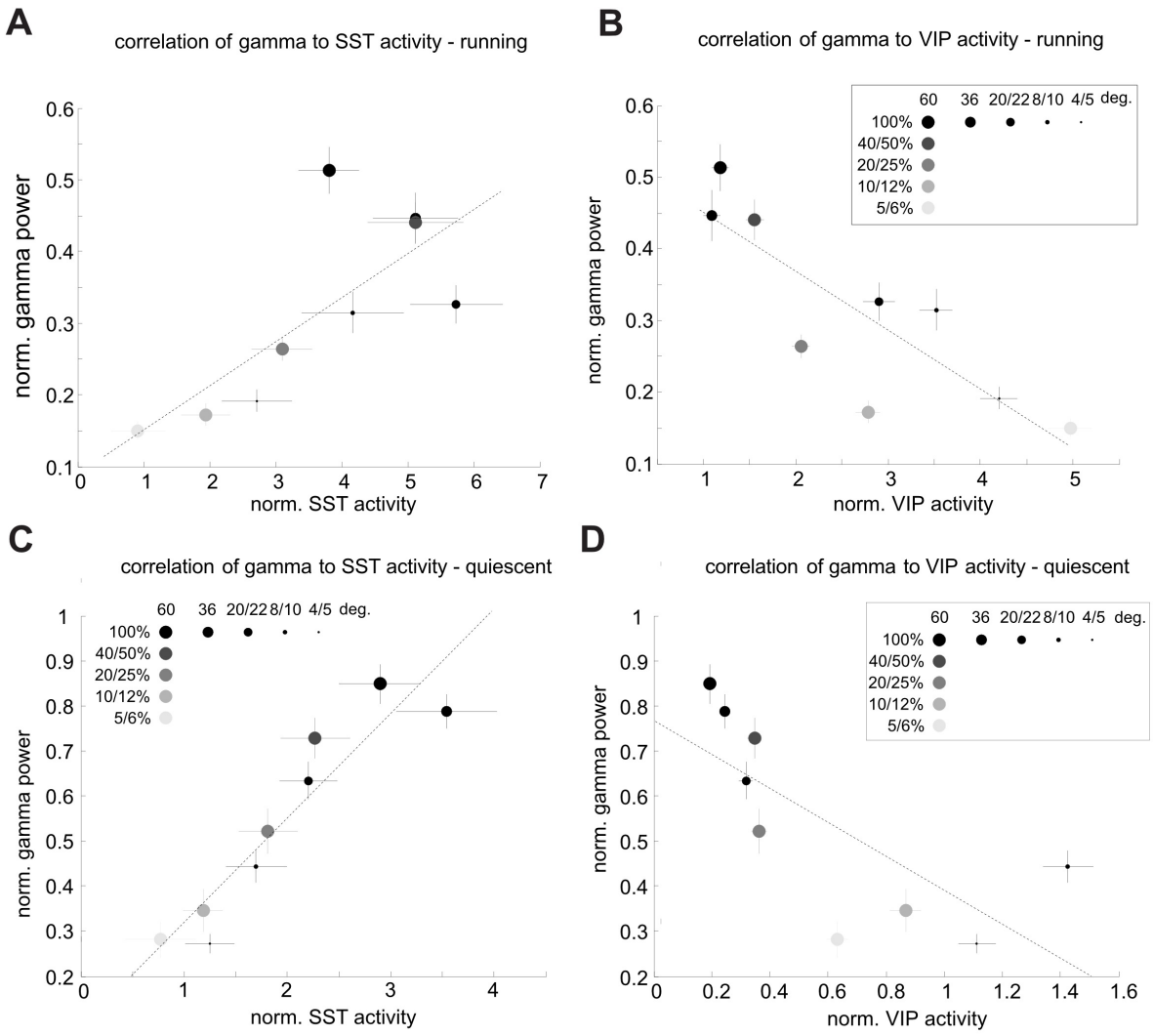

Figure S2: Opposing correlation of SST- and VIP-neuron activity with gamma power. A: Plot of averaged normalized gamma power in the running condition vs. averaged normalized SST-cell activity (deconvolved event-rate/mean), recorded via 2-photon imaging in a different set of animals across similar conditions. Different shades of gray represent different contrast levels and different symbol sizes represent different stimulus sizes. Dashed line is a linear fit of the data. SST-cell activity strongly correlates with gamma power ($r = 0.76$, $p = 0.019$). **B:** Same as A, except for normalized VIP cell activity. VIP activity is strongly anti-correlated with gamma power ($r = -0.84$, $p = 0.005$). **C:** Same as A, except in the quiescent state. SST-cell activity is strongly correlated to gamma power ($r = 0.93$, $p<0.001$). **D:** Same as B, except in the quiescent state. VIP activity is strongly anti-correlated to gamma power ($r = -0.73$, $p = 0.024$).

Figure S3 – related to Figure 2

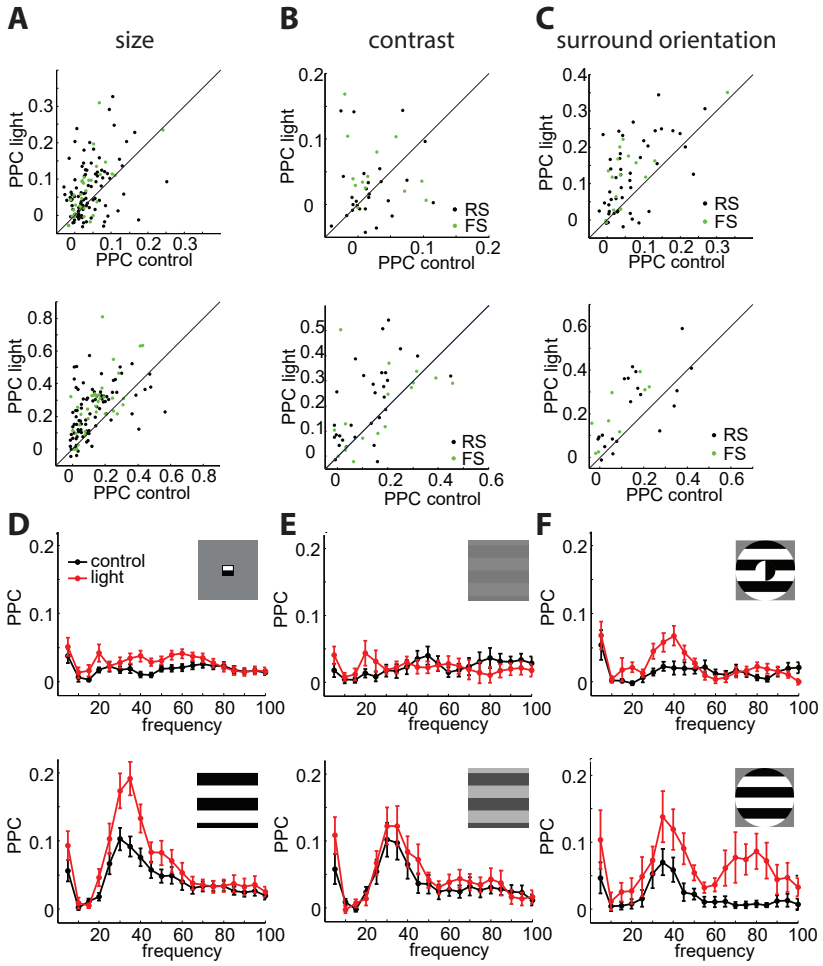

Fig. S3. Effects of VIP inactivation on locking of single RS and FS units. A: Top: scatter plot of PPC values for single RS (black, n = 90 units, $p < 0.001$, Wilcoxon signed rank test) and FS (green, n = 33 units, $p = 0.0015$, Wilcoxon signed rank test) units in response to small (4˚) stimuli in control condition versus VIP suppression. Bottom: scatter plot of PPC values for single RS (black, n = 87 units, $p < 0.001$, Wilcoxon signed rank test) and FS (green, n = 35 units, $p < 0.001$, Wilcoxon signed rank test) units in response to large (60˚) stimuli in control condition versus VIP suppression. **B:** Top: scatter plot of PPC values for single RS (black, n = 27 units, $p = 0.61$, Wilcoxon signed rank test) and FS (green, n = 13 units, $p = 0.31$, Wilcoxon signed rank test) units in response to low contrast (5%) stimuli in control condition versus VIP suppression. Bottom: scatter plot of PPC values for single RS (black, n = 30 units, $p = 0.001$, Wilcoxon signed rank test) and FS (green, n = 17 units, $p = 0.98$, Wilcoxon signed rank test) units in response to high contrast (80%) stimuli in control condition versus VIP suppression. **C:** Top: scatter plot of PPC values for single RS (black, n = 46 units, $p < 0.001$, Wilcoxon signed rank test) and FS (green, n = 15 units, $p < 0.001$, Wilcoxon signed rank test) units in response to cross surround stimuli in control condition versus VIP suppression. Bottom: scatter plot of PPC values for single RS (black, n = 21 units, $p = 0.04$, Wilcoxon signed rank test) and FS (green, n = 9 units, $p = 0.004$, Wilcoxon signed rank test) units in response to iso surround (0˚ offset) stimuli in control condition versus VIP suppression. **D:** Top: average PPC spectra for L2/3 FS units with (red) and without (black) suppression of VIP neurons (n = 30 units) for small (4˚) stimuli. Bottom: average PPC spectra for L2/3 FS units with (red) and without (black) suppression of VIP neurons (n = 32 units) for large (60˚) stimuli. **E:** Top: average PPC spectra for L2/3 FS units with (red) and without (black) suppression of VIP neurons (n = 13 units) for low contrast (5%) stimuli. Bottom: average PPC spectra for L2/3 FS units with (red) and without (black) suppression of VIP neurons (n = 17 units) for high contrast (80%) stimuli. **F:** top: average PPC spectra for L2/3 FS units with (red) and without (black) suppression of VIP neurons (n = 15 units) for cross surround (90˚ offset) stimuli. Bottom: average PPC spectra for L2/3 FS units with (red) and without (black) suppression of VIP neurons (n = 9 units) for iso surround (0˚ offset) stimuli.

Figure S4 – Related to Figure 1

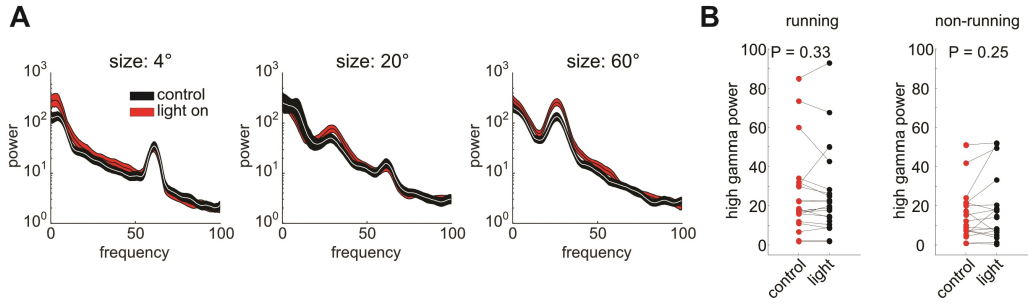

Figure S4. Effects of VIP inactivation on higher-frequency, narrowband, thalamic gamma (60Hz). A: Spectra for different size grating stimuli with (red) and without (black) inactivation of VIP neurons. VIP affects the visually induced 30Hz gamma band, but not the thalamically relayed 60Hz gamma band that is suppressed by large/high contrast stimuli. **B:** Plot comparing the LFP high gamma band power for blank stimuli in the running condition for control (black) and light (red) trials (n = 19 mice, p = 0.33, Wilcoxon signed rank test) Right: Plot comparing the LFP high gamma band power for blank stimuli in the quiescent condition for control (black) and light (red) trials (n = 18 mice, p = 0.25, Wilcoxon signed rank test).

Figure S5 – related to Figure 4

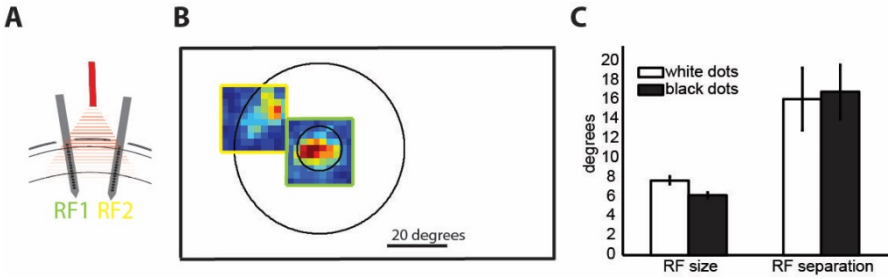

Figure S5. Receptive field mapping procedure for coherence measurement. A: Schematic of the multielectrode array recording configuration with two laminar arrays in distant sites (530 ± 90 µm apart, histology from *n* = 7 mice) corresponding to two separate retinotopic locations (RF1 (green) and RF2 (yellow), 15° ± 6° of visual angle separation, *n* = 10mice). Red triangle denotes wide illumination with optogenetic light delivered from a fiber located above the two recording sites. **B:** Two sparse noise mapped RFs (redder colors denote higher firing rates), one from electrode 1 (green frame), one from electrode 2 (yellow frame) superimposed on the outline of the center and surround of the visual stimulus used for the coherence analysis (Figure 4). Large outer frame is approximately the size of the stimulation monitor. **C:** average RF size (2 standard deviations of Gaussian fit to RF) and average separation of center and surround fields, separately for fields mapped with white and black sparse noise, *n* = 8 mice.

Figure S6 – related to Figure 5

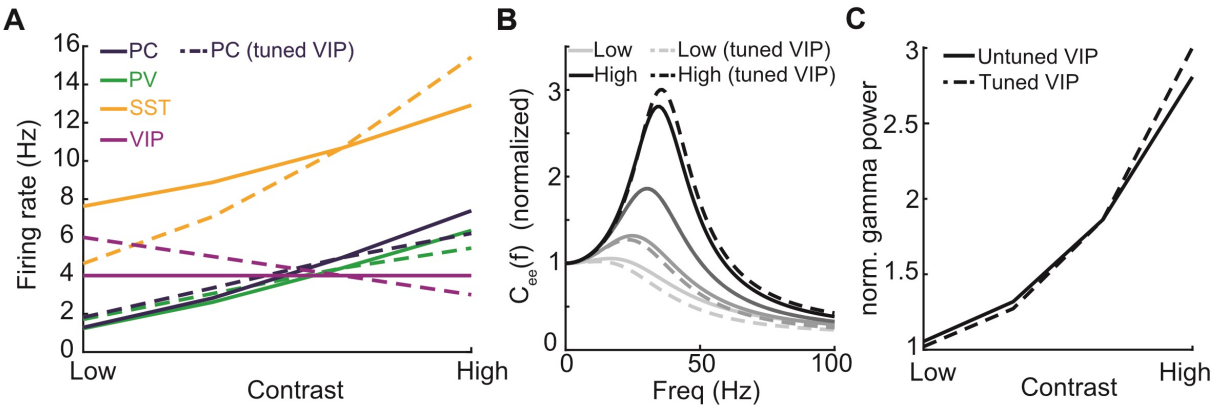

Figure S6. Modulation of gamma power in the presence of untuned and tuned VIP neurons. **A:** Average firing rates across different contrast levels across the populations for the mean-field theory as a function of contrast with untuned (solid) and tuned (dashed) VIP neurons. **B:** Normalized power spectrum from the mean-field model as a function of contrast for untuned (solid) and tuned (dashed) VIP neurons. **C:** Normalized gamma power taken from the power spectrum of panel B.

Methods S1. Linear response theory to find steady state firing rates, power spectrum and cross-spectrum of spike trains, and mean field theory, Related to the smooth lines in Figures 5, 6 and S6, and STAR Methods.

We solve for the steady state firing rates via the self-consistency relationship

$$r_i = r_i\left(\mu_i^{\text{eff}}, \sigma_i\right),$$

where

$$\mu_i^{\text{eff}} = E_L + \mu_{i,\text{bg}} + c\mu_{i,\text{stim}} + \mu_{i,v} + \sum_j \left(\int_{-\infty}^{\infty} J_{ij}(t)\, dt\right) W_{ij} r_j, \text{and}$$

$$\sigma_i = \sqrt{\left(\sigma_{i,\text{bg}}^2 + c\sigma_{i,\text{stim}}^2 + \sigma_{i,v}^2 + \sigma_{gl}^2\right) \cdot 2\tau_m},$$

for $i = 1, \ldots, N$ using standard methods developed in [1,2] for a nonlinear integrate-and-fire neuron.

We seek to understand the cross-covariance function of neuron i and j spike trains: $\mathbf{C}_{ij}(s) = \langle (y_i(t) - r_i)\left(y_j(t+s) - r_j\right)\rangle$. To do this, we follow previous work [3–6] and linearize each neuron's spike train around $\mathbf{y}_i^0$, a realization of the spiking output in the absence of recurrent connections. More specifically, by assuming weak synaptic connections $\mathbf{W}_{ij}$ and a bandlimited global noise process, we approximate the spike response from neuron i as

$$\tilde{\mathbf{y}}_i(\omega) = \tilde{\mathbf{y}}_i^0(\omega) + \widetilde{\mathbf{A}}_i(\omega)\left[\sigma_{gl}\sqrt{2\tau_m}\tilde{\boldsymbol{\eta}}_{gl}(\omega) + \textstyle\sum_j \mathbf{W}_{ij}\tilde{\mathbf{J}}_{ij}(\omega)\tilde{\mathbf{y}}_j(\omega)\right],$$

where $\tilde{\mathbf{y}}_i(\omega)$ is the zero mean Fourier transform of the spike train, $\tilde{f}$ denotes the Fourier transform of the other quantities, and $\widetilde{\mathbf{A}}_i(\omega)$ is the linear response of the postsynaptic neuron [7]. Solving for $\tilde{\mathbf{y}}(\omega)$ yields

$$\tilde{\mathbf{y}}(\omega) = \left(\mathbf{I} - \mathbf{K}(\omega)\right)^{-1}\left[\tilde{\mathbf{y}}^0(\omega) + \sigma_{gl}\sqrt{2\tau_m}\tilde{\boldsymbol{\eta}}_{gl}(\omega)\right],$$

where $\mathbf{I}$ is the identity matrix, $\mathbf{K}(\omega) = \widetilde{\mathbf{A}}(\omega)\left(\widetilde{\mathbf{W}} \odot \tilde{\mathbf{J}}(\omega)\right)$ and $\widetilde{\mathbf{A}}(\omega)$ is a diagonal matrix with entries $\widetilde{\mathbf{A}}_i(\omega)$. Writing the Fourier transform of $\mathbf{C_{ij}}(s)$ as $\tilde{\mathbf{C}}_{ij}(\omega)$, it follows that

$$\begin{aligned}
\tilde{\mathbf{C}}(\omega) &= \langle \tilde{\mathbf{y}}(\omega)\tilde{\mathbf{y}}^*(\omega)\rangle, \\
&= \left(\mathbf{I} - \mathbf{K}(\omega)\right)^{-1}\left[\langle \tilde{\mathbf{y}}^0(\omega)\tilde{\mathbf{y}}^{0*}(\omega)\rangle + \sigma_{gl}^2 2\tau_m \widetilde{\mathbf{A}}(\omega)\langle \tilde{\boldsymbol{\eta}}_{gl}(\omega)\tilde{\boldsymbol{\eta}}_{gl}^*(\omega)\rangle \widetilde{\mathbf{A}}^*(\omega)\right]\left(\mathbf{I} - \mathbf{K}^*(\omega)\right)^{-1}, \\
&= \left(\mathbf{I} - \mathbf{K}(\omega)\right)^{-1}\left[\tilde{\mathbf{C}}^0(\omega) + \sigma_{gl}^2 2\tau_m \langle \tilde{\eta}_{gl}(\omega)\tilde{\eta}_{gl}^*(\omega)\rangle \widetilde{\mathbf{A}}(\omega)\mathbf{1}\widetilde{\mathbf{A}}^*(\omega)\right]\left(\mathbf{I} - \mathbf{K}^*(\omega)\right)^{-1},
\end{aligned}$$

where $\tilde{\mathbf{y}}^*$ denotes the conjugate transpose, $\mathbf{1}$ is a matrix of ones, and $\tilde{\mathbf{C}}^0(\omega)$ is a diagonal matrix of the power spectrums of the baseline spike trains.

We now develop a mean-field theory to significantly compress the previous $N \times N$ matrices for the case where a visual stimulus only evokes the center retinotopic location, yielding matrices that are 3×3. The extension to larger visual stimuli evoking the discrete surround populations follows in a similar manner. Further, we focus on the case of a network with a fixed in-degree for each neuron of a specific population, though it can be generalized to account for additional network configurations. Denote N_a as the relative sizes of each population, with $a = e\ (\text{PC}),\ p\ (\text{PV}), \text{and}\ s\ (\text{SST})$.

We start the derivation for the population-average pairwise covariance matrix by averaging the spike response equation in the Fourier domain

$$\frac{1}{N_a}\sum_{i\in a}\tilde{\mathbf{y}}_{\boldsymbol{i}}(\omega) = \frac{1}{N_a}\sum_{i\in a}\left[\tilde{\mathbf{y}}_i^0(\omega) + \sigma_{gl}^2 2\tau_m \widetilde{\mathbf{A}}_i(\omega)\tilde{\eta}_{gl}(\omega) + \widetilde{\mathbf{A}}_i(\omega)\sum_j \mathbf{W}_{ij}\tilde{\mathbf{J}}_{ij}(\omega)\tilde{\mathbf{y}}_j(\omega)\right],$$

$$= \frac{1}{N_a}\sum_{i\in a}\tilde{\mathbf{y}}_i^0(\omega) + \sigma_{gl}^2 2\tau_m \tilde{\eta}_{gl}(\omega)\cdot\frac{1}{N_a}\sum_{i\in a}\widetilde{\mathbf{A}}_i(\omega) + \frac{1}{N_a}\sum_{i\in a}\left[\widetilde{\mathbf{A}}_i(\omega)\sum_j \mathbf{W}_{ij}\tilde{\mathbf{J}}_{ij}(\omega)\tilde{\mathbf{y}}_j(\omega)\right].$$

We can break the third sum in the last line by the population j belongs to, noting that

$$\frac{1}{N_a}\left[\sum_{i\in a}\sum_{j\in b}\widetilde{\mathbf{A}}_i(\omega)\mathbf{W}_{ij}\tilde{\mathbf{J}}_{ij}(\omega)\tilde{\mathbf{y}}_j(\omega)\right] \approx \frac{1}{N_a}\left[\widetilde{\mathbf{A}}_a(\omega)w_{ab}p_{ab}N_a\tilde{\mathbf{J}}_{ab}(\omega)\sum_{j\in b}\tilde{\mathbf{y}}_j(\omega)\right]$$

$$= (w_{ab}p_{ab}N_b)\widetilde{\mathbf{A}}_a(\omega)\tilde{\mathbf{J}}_{ab}(\omega)\widehat{\tilde{\mathbf{y}}}_b(\omega),$$

where

$$\widehat{\tilde{\mathbf{y}}}_b(\omega) = \frac{1}{N_b}\sum_{j\in b}\tilde{\mathbf{y}}_j(\omega)$$

denotes the Fourier transform of the concatenated spike trains from each population,

$$\hat{y}_b = \frac{1}{N_b}\sum_{j\in b} y_j(t).$$

The first line follows from the fact that for a fixed in-degree network, as considered here, a neuron in population b makes on average $p_{ab}N_a$ connections to a neuron in population a, the synaptic kernel $\tilde{\mathbf{J}}_{ij}(\omega)$ is the same for all neurons from population b to a and $\widetilde{\mathbf{A}}_i(\omega)$ is the same for all neurons in the same population. Alternatively, one could consider a fixed out-degree network, where the number of connections is $p_{ab}N_a$ exactly, but in case, one would have to consider the average of $\widetilde{\mathbf{A}}_i(\omega)$across the population. The coefficient $w_{ab}p_{ab}N_b$ is the effective connectivity from population b to a. Designating the effective connectivity matrix as

$$M = \begin{bmatrix} w_{ee}p_{ee}N_e & w_{ep}p_{ep}N_p & w_{es}p_{es}N_s \\ w_{pe}p_{pe}N_e & w_{pp}p_{pp}N_p & w_{ps}p_{ps}N_s \\ w_{se}p_{se}N_e & 0 & 0 \end{bmatrix} = \begin{bmatrix} M_{ee} & M_{ep} & M_{es} \\ M_{pe} & M_{pp} & M_{ps} \\ M_{se} & 0 & 0 \end{bmatrix},$$

we can write

$$\widehat{\tilde{\mathbf{y}}}_a(\omega) = \widehat{\tilde{\mathbf{y}}}_a^0(\omega) + \sigma_{gl}^2 2\tau_m\tilde{\eta}_{gl}(\omega)\widetilde{\mathbf{A}}_a(\omega) + \widetilde{\mathbf{A}}_a(\omega)\sum_b \mathbf{M}_{ab}\tilde{\mathbf{J}}_{ab}(\omega)\widehat{\tilde{\mathbf{y}}}_b(\omega).$$

Proceeding as before yields

$$\hat{\tilde{\mathbf{C}}}(\omega) = \langle\hat{\tilde{\mathbf{y}}}(\omega)\hat{\tilde{\mathbf{y}}}^*(\omega)\rangle,$$

$$= \left(I - \widehat{\tilde{\mathbf{K}}}(\omega)\right)^{-1}\left[\langle\tilde{\mathbf{y}}^0(\omega)\tilde{\mathbf{y}}^{0*}(\omega)\rangle + \sigma_{gl}^2 2\tau_m\widetilde{\mathbf{A}}(\omega)\langle\tilde{\boldsymbol{\eta}}_{gl}(\omega)\tilde{\boldsymbol{\eta}}_{gl}^*(\omega)\rangle\widetilde{\mathbf{A}}^*(\omega)\right]\left(I - \widehat{\tilde{\mathbf{K}}}^*(\omega)\right)^{-1},$$

$$= \left(I - \widehat{\mathbf{K}}(\omega)\right)^{-1} \left[\hat{\tilde{\mathbf{C}}}^{\mathbf{0}}(\omega) + \sigma_{gl}^2 2\tau_m \langle \tilde{\eta}_{gl}(\omega)\tilde{\eta}_{gl}^*(\omega)\rangle \hat{\tilde{\mathbf{A}}}(\omega)\mathbf{1}\hat{\tilde{\mathbf{A}}}^*(\omega)\right] \left(I - \widehat{\mathbf{K}}^*(\omega)\right)^{-1},$$

with

$$\widehat{\mathbf{K}}(\omega) = \hat{\tilde{\mathbf{A}}}(\omega)\left(\mathbf{M} \odot \hat{\tilde{\mathbf{J}}}(\omega)\right)$$

where

$$\hat{\tilde{\mathbf{A}}}(\omega) = \mathrm{diag}\left(\tilde{\mathbf{A}}_e(\omega), \tilde{\mathbf{A}}_p(\omega), \tilde{\mathbf{A}}_s(\omega)\right),$$
$$\hat{\tilde{\mathbf{J}}}(\omega) = \begin{bmatrix} \tilde{\mathbf{J}}_{ee}(\omega) & \tilde{\mathbf{J}}_{ep}(\omega) & \tilde{\mathbf{J}}_{es}(\omega) \\ \tilde{\mathbf{J}}_{pe}(\omega) & \tilde{\mathbf{J}}_{pp}(\omega) & \tilde{\mathbf{J}}_{ps}(\omega) \\ \tilde{\mathbf{J}}_{se}(\omega) & \tilde{\mathbf{J}}_{sp}(\omega) & \tilde{\mathbf{J}}_{ss}(\omega) \end{bmatrix}, \text{and}$$
$$\hat{\tilde{\mathbf{C}}}^0(\omega) = \mathrm{diag}\left(\frac{1}{N_e}\tilde{\mathbf{C}}_{ee}^0(\omega), \frac{1}{N_p}\tilde{\mathbf{C}}_{pp}^0(\omega), \frac{1}{N_s}\tilde{\mathbf{C}}_{ss}^0(\omega)\right).$$

The diagonal matrix $\hat{\tilde{\mathbf{C}}}^0(\omega)$ follows from the calculation

$$\hat{\tilde{\mathbf{C}}}_{aa}^0(\omega) = \langle \hat{\tilde{\mathbf{y}}}_a(\omega)\hat{\tilde{\mathbf{y}}}_a^*(\omega)\rangle = \langle \frac{1}{N_a}\sum_{i\in a}\tilde{y}_i^0(\omega) \cdot \frac{1}{N_a}\sum_{j\in a}\tilde{y}_j^{0*}(\omega)\rangle$$
$$= \frac{1}{N_a^2}\sum_{i\in a}\langle \tilde{y}_i^0(\omega)\tilde{y}_i^{0*}(\omega)\rangle = \frac{1}{N_a}\tilde{\mathbf{C}}_{aa}^0(\omega),$$

where the equality follows from the fact that like the linear response function, the neurons in a fixed in-degree network have the same spike train power spectrum across populations. This calculation yields a block-wise averaged power and cross-spectrum matrix

$$\hat{\tilde{\mathbf{C}}}(\omega) = \begin{bmatrix} \tilde{\mathbf{C}}_{ee}(\omega) & \tilde{\mathbf{C}}_{ep}(\omega) & \tilde{\mathbf{C}}_{es}(\omega) \\ \tilde{\mathbf{C}}_{pe}(\omega) & \tilde{\mathbf{C}}_{pp}(\omega) & \tilde{\mathbf{C}}_{ps}(\omega) \\ \tilde{\mathbf{C}}_{se}(\omega) & \tilde{\mathbf{C}}_{sp}(\omega) & \tilde{\mathbf{C}}_{ss}(\omega) \end{bmatrix},$$

where

$$\hat{\tilde{\mathbf{C}}}_{ab}(\omega) \approx \frac{1}{N_a}\frac{1}{N_a}\sum_{i\in a}\sum_{j\in b}\hat{\tilde{\mathbf{C}}}_{ij}(\omega).$$

This theory can be extended to account for global noise that takes the form of Gaussian white noise (with infinite variance). Following previous work [4], this results in the following equation for $\hat{\tilde{\mathbf{C}}}(\omega)$

$$\hat{\tilde{\mathbf{C}}}(\omega) = \left(I - \widehat{\mathbf{K}}(\omega)\right)^{-1} \left[\hat{\tilde{\mathbf{C}}}^{\mathbf{0}}(\omega) + \sigma_{gl}^2 2\tau_m \langle \tilde{\eta}_{gl}(\omega)\tilde{\eta}_{gl}^*(\omega)\rangle \hat{\tilde{\mathbf{A}}}(\omega)\mathbf{1}\hat{\tilde{\mathbf{A}}}^*(\omega) - \sigma_{gl}^2 2\tau_m \left|\hat{\tilde{\mathbf{A}}}_N(\omega)\right|^2\right] \left(I - \widehat{\mathbf{K}}^*(\omega)\right)^{-1},$$

where

$$\widehat{\widetilde{\mathbf{A}}}_N(\omega) = \mathrm{diag}\left(\frac{1}{N_e}\widetilde{\mathbf{A}}_e(\omega), \frac{1}{N_p}\widetilde{\mathbf{A}}_p(\omega), \frac{1}{N_s}\widetilde{\mathbf{A}}_s(\omega)\right).$$

We note that for the parameters considered (i.e., the magnitude of the global noise term is small relative to the independent noise), this correction term as a minimal effect on $\hat{\tilde{\mathbf{C}}}(\omega)$, being orders of magnitude smaller than the other terms in this equation.

To estimate the linear response functions and the spike train power spectrum for each population, we first need the population-average steady state firing rates,

$$r_a = \frac{1}{N_a}\sum_{i\in a} r_i.$$

Using the effective connectivity across populations, we can use the same self-consistency relationship as the non-average quantities to find the population average steady-state firing rates, namely

$$r_a = r_a\left(\mu_a^{\mathrm{eff}}, \sigma_a\right),$$

where

$$\mu_a^{\mathrm{eff}} = E_L + \mu_{a,\mathrm{bg}} + c\mu_{a,\mathrm{stim}} + \mu_{a,v} + \sum_b \left(\int_{-\infty}^{\infty} \mathbf{J}_{ab}(t)\, dt\right)\mathbf{M}_{ab} r_b, \text{ and}$$

$$\sigma_a = \sqrt{\left(\sigma_{a,\mathrm{bg}}^2 + c\sigma_{a,\mathrm{stim}}^2 + \sigma_{a,v}^2 + \sigma_{gl}^2\right)\cdot 2\tau_m}.$$

With these population rates, we can then apply the theory developed in [1,2] to

$$\tau_m \frac{dV_a}{dt} = -(V_a - E_L) + \psi(V_a) + \sigma_a \xi_a,$$

in order to numerically estimate $\widetilde{\mathbf{A}}_a(\omega)$ and $\tilde{\mathbf{C}}_{aa}^0(\omega)$. These terms will exactly match that of $\widetilde{\mathbf{A}}_i(\omega)$ and $\tilde{\mathbf{C}}_{ii}^0(\omega)$ for $i \in a$ of the full system when the network has a fixed in-degree. Otherwise, this method would estimate the average of these quantities across the population.

Finally, using the power spectrums for two excitatory populations $\left(\tilde{\mathbf{C}}_{e_1e_1}(\omega) \text{ and } \tilde{\mathbf{C}}_{e_2e_2}(\omega)\right)$ and their cross-spectrum $\left(\tilde{\mathbf{C}}_{e_1e_2}(\omega)\right)$, the coherence is taken to be

$$\mathrm{coherence}(\omega) = \frac{\left|\tilde{\mathbf{C}}_{e_1e_2}(\omega)\right|^2}{\tilde{\mathbf{C}}_{e_1e_1}(\omega)\cdot\tilde{\mathbf{C}}_{e_2e_2}(\omega)}.$$

Methods S2. LFP Power and Cross do not necessarily scale in finite size networks, Related to STAR Methods.

Work by [8] recently derived results showing that under certain assumptions power and coherence are intrinsically linked. However, such a result need not be the case [9,10], and indeed, does not follow from the theory above, where shifting the operating point (through changing contrast, VIP activation, cross vs. iso surround) results in the power and cross-spectrums to change in different ways. Thus, a change in power doesn't necessarily result in a change in coherence.

To highlight the differences in approaches, consider two excitatory populations ($\alpha \in \{e_1, e_2\}$) and assume homogeneity with

$$\begin{aligned}
\langle\, \tilde{y}_i(\omega)\tilde{y}_i^*(\omega)\rangle &= p(\omega), \quad \text{for } i \in \alpha \\
\left\langle\, \tilde{y}_i(\omega)\tilde{y}_j^*(\omega)\right\rangle &= c^w(\omega), \quad \text{for } i,j \in \alpha \text{ and } i \neq j \\
\left\langle\, \tilde{y}_i(\omega)\tilde{y}_j^*(\omega)\right\rangle &= c^b(\omega), \quad \text{for } i \in e_1 \text{ and } j \in e_2
\end{aligned}$$

where recall that $\tilde{y}_i(\omega)$ is the zero mean Fourier transform of the spike train, and ω is the frequency coordinate. In brief, $p(\omega)$ is the single neuron power spectrum, $c^w(\omega)$ is the within population pairwise cross spectrum and $c^b(\omega)$ is the between population pairwise spectrum.

The LFP power spectrum of population α is then

$$\begin{aligned}
\tilde{\mathbf{C}}_{\alpha\alpha}(\omega) &= \frac{1}{N_\alpha \cdot N_\alpha} \sum_{i\in\alpha}\sum_{j\in\alpha} \left\langle\, \tilde{y}_i(\omega)\tilde{y}_j^*(\omega)\right\rangle \\
&= \frac{1}{N^2}\left[\sum_{i\in\alpha} \langle\, \tilde{y}_i(\omega)\tilde{y}_i^*(\omega)\rangle + \sum_{i\in\alpha}\sum_{j\in\alpha, j\neq i} \left\langle\, \tilde{y}_i(\omega)\tilde{y}_j^*(\omega)\right\rangle\right] \\
&= \frac{1}{N^2}\left(N\, p(\omega) \;+\; N(N-1)c^w(\omega)\right) \\
&\approx \frac{p(\omega)}{N} + c^w(\omega),
\end{aligned}$$

where we have assumed $N_{e_1} = N_{e_2} = N$. Similarly, the cross spectrum between LFPs is

$$\begin{aligned}
\tilde{\mathbf{C}}_{e_1e_2}(\omega) &= \frac{1}{N_{e_1} \cdot N_{e_2}} \sum_{i\in e_1}\sum_{j\in e_2} \left\langle\, \tilde{y}_i(\omega)\tilde{y}_j^*(\omega)\right\rangle \\
&= \frac{1}{N^2}\left(N^2 c^b(\omega)\right) \\
&= c^b(\omega).
\end{aligned}$$

Finally, the coherence between LFPs is

$$\begin{aligned}
\text{coherence}(\omega) &= \frac{\left|\tilde{\mathbf{C}}_{e_1e_2}(\omega)\right|^2}{\tilde{\mathbf{C}}_{e_1e_1}(\omega) \cdot \tilde{\mathbf{C}}_{e_2e_2}(\omega)} \\
&= \frac{\left|c^b(\omega)\right|^2}{\left(\frac{p(\omega)}{N} + c^w(\omega)\right)^2}.
\end{aligned}$$

Our linear response calculations linearize the network dynamics about an operating point. This allows us to calculate $p(\omega)$, $c^w(\omega)$, and $c^b(\omega)$ using standard techniques from non-equilibrium statistical mechanics. In particular, the single neuron power spectrum $p(\omega)$ and pairwise cross spectrum $c(\omega)$ result from separate calculations where the linearity of interaction is needed for $c(\omega)$ yet not for $p(\omega)$. When we shift the operating point $p(\omega)$ and $c(\omega)$ change in different ways. Since for $N < \infty$ the coherence $\mathrm{coherence}(\omega)$ depends on both $p(\omega)$ and $c(\omega)$ then $\mathrm{coherence}(\omega)$ will not be invariant with a shift in the operating point.

However, other work [8,10,11] has assumed heuristically, or by construction, that

$$\tilde{\mathbf{C}}_{e_1e_2}(\omega) = \beta\tilde{\mathbf{C}}_{e_1e_1}(\omega), \text{and } \tilde{\mathbf{C}}_{e_1e_1}(\omega) = H(\omega) + \beta^2\tilde{\mathbf{C}}_{e_1e_1}(\omega),$$

which simplifies the coherence to be

$$\begin{aligned}\mathrm{coherence}(\omega) &= \frac{\left|\beta\tilde{C}_{e_1e_1}(\omega)\right|^2}{\tilde{C}_{e_1e_1}(\omega)\cdot\left(H(\omega) + \beta^2\tilde{C}_{e_1e_1}(\omega)\right)} \\ &= \frac{1}{1 + H(\omega)\left(\beta^2\tilde{C}_{e_1e_1}(\omega)\right)^{-1}}\,.\end{aligned}$$

As a result, this assumption implies that even with finite N, coherence and power will be intrinsically linked. Yet, our experimental observations show that such an assumption does not hold, at least across spatial locations in V1.

Table S1. Default neuronal parameters, Related to STAR Methods.

Parameter	Value	Description
N_{ex}	4000	number of excitatory neurons at location x
N_{px}	500	number of PV neurons at location x
N_{sx}	500	number of SST neurons at location x
N_{vx}	500	number of VIP neurons at location x
E_l	-60 mV	resting potential
V_{th}	20 mV	threshold potential
V_{re}	-75 mV	reset potential
τ_m	5.4 msec	membrane time constant
τ_s	0.6 msec	synaptic time constant
τ_{ref}	1.2 msec	refractory period
Δ_T	-50 mV	exponential shape parameter (soft threshold)
V_{lb}	-100 mV	lower bound for voltage
τ_{delay}	1.8 msec	Synaptic delay
$w = w_{ae}$	$0.48\ \mathrm{mV} \cdot \mathrm{msec}$	synaptic strength of excitatory connections
g	4	amplification of inhibitory connection strength
$w_{ap} = w_{as}$	$-gw$	synaptic strength of inhibitory connections
$[\mu_{e,bg}, \mu_{p,bg}, \mu_{s,bg}]$	$[3, 3, 7]$ mV	background mean
$[\sigma^2_{e,bg}, \sigma^2_{p,bg}, \sigma^2_{s,bg}]$	$[2.1, 2.1, 3]$ mV	background standard deviation
$[\mu_{e,stim}, \mu_{p,stim}, \mu_{s,stim}]$	$[3, 3, 0]$ mV	stimulus mean
$[\sigma^2_{e,stim}, \sigma^2_{p,stim}, \sigma^2_{s,stim}]$	$[2.1, 2.1, 0]$ mV	stimulus standard deviation
σ_{gl}	0.25 mV	global noise standard deviation
c	0.5-1.0	contrast weight
r_v	0-14 Hz	firing rate of VIP neurons
$[w_{e,v}, w_{p,v}, w_{s,v}]$	$[0,0,-6.4]$	strength of VIP connections

Table S2. Probability of connections p_{ab} (from population b to a; columns presynaptic, rows postsynaptic), Related to STAR Methods.

	Same spatial location			Different spatial location	
	PC	PV	SST	PC (iso)	PC (cross)
PC	0.07	0.15	0.10	0.02	0.01
PV	0.05	0.10	0.10	0.03	0.005
SST	0.10	0.00	0.00	0.08	0.05

References

1. Richardson, M.J.E. (2007). Firing-rate response of linear and nonlinear integrate-and-fire neurons to modulated current-based and conductance-based synaptic drive. Physical Review E - Statistical, Nonlinear, and Soft Matter Physics *76*, 1–15. 10.1103/PhysRevE.76.021919.

2. Richardson, M.J.E. (2008). Spike-train spectra and network response functions for non-linear integrate-and-fire neurons. Biological Cybernetics *99*, 381–392. 10.1007/s00422-008-0244-y.

3. Doiron, B., Lindner, B., Longtin, A., Maler, L., and Bastian, J. (2004). Oscillatory activity in electrosensory neurons increases with the spatial correlation of the stochastic input stimulus. Physical Review Letters *93*, 048101–1. 10.1103/PhysRevLett.93.048101.

4. Lindner, B., Doiron, B., and Longtin, A. (2005). Theory of oscillatory firing induced by spatially correlated noise and delayed inhibitory feedback. Physical Review E - Statistical, Nonlinear, and Soft Matter Physics *72*, 1–14. 10.1103/PhysRevE.72.061919.

5. Trousdale, J., Hu, Y., Shea-Brown, E., and Josić, K. (2012). Impact of Network Structure and Cellular Response on Spike Time Correlations. PLoS Computational Biology *8*, e1002408. 10.1371/journal.pcbi.1002408.

6. Ocker, G.K., Litwin-Kumar, A., and Doiron, B. (2015). Self-Organization of Microcircuits in Networks of Spiking Neurons with Plastic Synapses. PLoS Computational Biology *11*, 1–40. 10.1371/journal.pcbi.1004458.

7. Gardiner, C. (2009). Stochastic Methods: A Handbook for the Natural and Social Sciences (Springer Berlin Heidelberg).

8. Schneider, M., Broggini, A.C., Dann, B., Tzanou, A., Uran, C., Sheshadri, S., Scherberger, H., and Vinck, M. (2021). A mechanism for inter-areal coherence through communication based on connectivity and oscillatory power. Neuron, 1–18. 10.1016/j.neuron.2021.09.037.

9. de la Rocha, J., Doiron, B., Shea-Brown, E., Josić, K., and Reyes, A. (2007). Correlation between neural spike trains increases with firing rate. Nature *448*, 802–806. 10.1038/nature06028.

10. Josić, K., Shea-Brown, E., Doiron, B., and de la Rocha, J. (2009). Stimulus-dependent correlations and population codes. Neural computation *21*, 2774–2804. 10.1162/neco.2009.10-08-879.

11. Abbott, L.F., and Dayan, P. (1999). The effect of correlated variability on the accuracy of a population code. Neural Computation *11*, 91–101. 10.1162/089976699300016827.